## RSC Advances



This is an *Accepted Manuscript*, which has been through the Royal Society of Chemistry peer review process and has been accepted for publication.

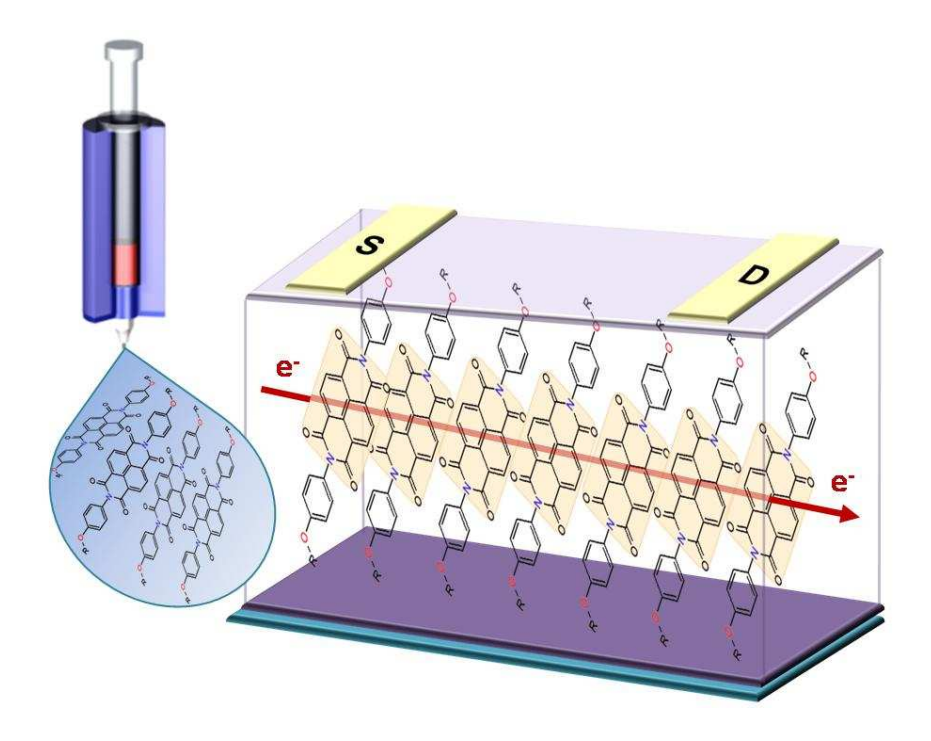
Accepted Manuscripts are published online shortly after acceptance, before technical editing, formatting and proof reading. Using this free service, authors can make their results available to the community, in citable form, before we publish the edited article. This Accepted Manuscript will be replaced by the edited, formatted and paginated article as soon as this is available.

You can find more information about *Accepted Manuscripts* in the **Information for Authors**.

Please note that technical editing may introduce minor changes to the text and/or graphics, which may alter content. The journal's standard <u>Terms & Conditions</u> and the <u>Ethical guidelines</u> still apply. In no event shall the Royal Society of Chemistry be held responsible for any errors or omissions in this *Accepted Manuscript* or any consequences arising from the use of any information it contains.



Page 1 of 31



New alkoxy-substituted naphthalene bisimides exhibit strong tendency to form supramolecularly ordered layers and yield air operating n-channel field effect transistors.

# New semiconducting naphthalene bisimides N-substituted with alkoxyphenyl groups: spectroscopic, electrochemical, structural and electrical properties

Renata Rybakiewicz,<sup>a</sup> Izabela Tszydel,<sup>b</sup> Joanna Zapala,<sup>c,d</sup> Lukasz Skorka,<sup>a</sup> Damian Wamil,<sup>a</sup> David Djurado,<sup>d</sup> Jacques Pécaut,<sup>e</sup> Jacek Ulanski,<sup>b</sup> Malgorzata Zagorska,<sup>a,\*</sup> and Adam Pron<sup>a,\*\*</sup>

<sup>a</sup>Faculty of Chemistry, Warsaw University of Technology, Noakowskiego 3, 00664 Warsaw, Poland

<sup>b</sup>Department of Molecular Physics, Technical University of Lodz, Zeromskiego 116, 90-924 Lodz, Poland

<sup>c</sup>Institute of Physical Chemistry, Polish Academy of Sciences, Kasprzaka 44/52, 01224 Warsaw, Poland

<sup>d</sup>CEA Grenoble, INAC/SPrAM (UMR 5819, CEA-CNRS-Univ. J. Fourier-Grenoble 1), LEMOH, 17 Rue des Martyrs, 38054 Grenoble Cedex 9, France

<sup>e</sup>CEA Grenoble, INAC/SCIB, 17 Rue des Martyrs, 38054 Grenoble Cedex 9, France

**ABSTRACT** Three new naphthalene bisimides with alkoxyphenyl N-substituents (abbreviated as NBI-4-n-ORPhs, where R = butyl, hexyl or octyl group) were synthesized as well as spectroscopically, electrochemically and structurally characterized. DFT calculations predicted a high value of the electron affinity (EA) and a low lying LUMO level for these compounds. These findings were corroborated by cyclic voltammetry which yielded the experimental |EA| values of ca. of 4.11 eV – 4.12 eV and the ionization potential (IP) values in the range of 6.33 eV – 6.37 eV. When solution processed, the investigated semiconductors formed highly ordered and oriented layers, whose supramolecular organizations were derived from the structures determined for the corresponding single crystals. In particular  $\pi$ -stacked molecules formed molecular rows with stacking direction parallel to the substrate on which the films were deposited. As determined by X–ray diffraction studies, zone-casting technique turned out to be especially suitable for depositing layers of very good structural homogeneity, desired orientation of the molecules and high coherence length. High |EA| values of NBI-4-n-ORPhs together with their ordered

supramolecular organization in zone-cast layers made these new semiconductors very good candidates for fabrication of n-channel field effect transistors (FETs). The devices with Parylene C dielectric reached the electron mobility up to 0.05 cm<sup>2</sup>V<sup>-1</sup>s<sup>-1</sup> in air operating conditions.

**KEYWORDS** alkoxyphenyl substituted naphthalene bisimides, electrochemistry, DFT calculations, single crystals structure, thin layers and zone-casting, high electron mobility, n-channel organic field effect transistors

### Introduction

Arylene bisimide derivatives constitute an important class of compounds which show, in addition to their diversified covalent and supramolecular chemistry, an interesting reversible electrochemical behavior. Appropriately functionalized bisimides can serve as dyes. They also show semiconducting properties and for this reason they have been most intensively studied as components of active layers in organic electronic devices, mainly n-channel field effect transistors and ambipolar transistors. Both low molecular mass and polymeric bisimides are being used for this purpose.

Naphthalene and perylene bisimides N-substituted with alkyl groups are solution processable which is a significant advantage. However, n-channel transistors fabricated from these compounds fail to operate in air because their electron affinity |EA| is too low. A popular method of increasing the |EA| value in this family of compounds is their aromatic core functionalization with electron withdrawing groups. <sup>13</sup> An evident drawback of this procedure is a complicated (in some cases) reaction pathway, in addition involving reactions which are not completely selective. <sup>13</sup> Alternatively, imide nitrogen functionalization can be applied, which usually is simpler. For example, changing alkyl N-substituent for their highly fluorinated or perfluorinated analogues leads to an increase of |EA| by *ca* 150 meV, but frequently on the expense of solution processability. <sup>15-17</sup>

In one of our previous papers we have demonstrated that the redox properties of naphthalene bisimides are much more sensitive to aryl *versus* alkyl substitution than their perylene analogues.<sup>18</sup> For example alkylphenyl substituted napthalene bisimides show |EA| values higher by 60 to 90 meV as compared to their alkyl substituted derivatives.<sup>18</sup> This effect is not observed in perylene bisimides, where fluorination of the phenyl ring is required to increase

|EA|. Thus, using alkylphenyl substituted naphthalene bisimides n-channel transistors showing high charge carriers mobility were fabricated. 21

In this paper we demonstrate that alkoxyphenyl N-substituted naphthalene bisimides also constitute a promising class of solution processable organic semiconductors. We also describe a joint experimental and theoretical investigation of their spectroscopic and electrochemical properties. Then we discuss the effect of the N-substituent lengths on their supramolecular organization in single crystals and in thin layers deposited on glass using the so called "zone-casting" technique. Finally we test them as components of active layers in air operating n-channel field effect transistors easy to fabricate by zone-casting. Such new materials, showing good charge carriers mobility, are still highly demanded, since they are scarcer than those suitable for the p-channel devices. This is especially important for the fabrication of the so called "complementary circuits" where comparable performance of n- and p-channel transistors must be assured.

One of the investigated compounds, namely the bisimide with butoxyphenyl substituents, was already reported in the literature.<sup>23</sup> It was studied as a model compound of polyimides containing naphthalene moiety, however its electrochemical, structural and semiconducting properties were not investigated. Moreover, it was synthesized using a different and more complicated pathway.

## **Experimental section**

**Synthesis.** All three compounds studied were prepared via a condensation reaction between naphthalene dianhydride and the corresponding p-alkoxyphenylamine (commercially available) as shown in *Scheme 1*.

**Scheme 1** Synthesis of N,N'-bis(4-alkoxyphenyl)-1,4,5,8-naphthalene tetracarboxylic-1,4:5,8-bisimides, abbreviated as NBI-4-n-OBuPh (1), NBI-4-n-OHePh (2) and NBI-4-n-OOcPh (3)

 $R = n-C_4H_9$  (NBI-4-n-OBuPh);  $n-C_6H_{13}$  (NBI-4-n-OHePh);  $n-C_8H_{17}$  (NBI-4-n-OOcPh)

General procedure of the synthesis of N,N'-bis(4-alkoxyphenyl)-1,4,5,8-naphthalene tetracarboxylic-1,4:5,8-bisimides. 4.2 mmol of a given p-alkoxyaniline and 2.0 mmol (0.439 g) of zinc acetate dihydrate were added to a stirred suspension of 2.0 mmol (0.536 g) of 1,4,5,8-naphthalenetetracarboxylic acid bisanhydride in 25 ml of dry 1-methyl-2-pyrrolidinone (NMP). The resulting mixture was stirred at 180°C for 4 hours under argon atmosphere, and then poured into 100 ml of cold water. The obtained precipitate was filtered off, washed with water and acetone and then dried in a desiccator. The obtained bisimides were purified using a chromatographic column (silica gel, chloroform + 1 vol% triethylamine). The resulting material was crystallized from chloroform.

**N,N'-Bis(4-n-butoxyphenyl)-1,8:4,5-naphthalenetetracarboxylic** (NBI-4-n-OBuPh), orange solid, reaction yield of 60%.  $^{1}$ H NMR (CDCl<sub>3</sub>, 400 MHz, ppm): 8.83 (s, 4H); 7.23 (d, 4H, J = 8.8 Hz); 7.08 (d, 4H, J = 8.8 Hz); 4.03 (t, 4H, J = 6.4 Hz); 1.85-1.78 (m, 4H); 1.54-1.48 (m, 4H); 1.01 (t, 6H, J = 7.6 Hz).  $^{13}$ C NMR (CDCl<sub>3</sub>, 100 MHz): 163.17; 159.52; 131.38; 129.30;127.15; 127.03; 126.64; 115.36; 67.95; 31.29; 19.29; 13.87. FTIR (KBr, cm<sup>-1</sup>): 3465, 3417; 3083, 2923, 2869, 1717, 1669, 1507, 1443, 1345, 1243, 1185, 1167, 980, 872, 829, 752, 743. Elemental analysis: Calcd for  $C_{34}H_{30}N_{2}O_{6}$ : C, 72.58, H, 5.37, N, 4.98. Found: C, 72.60, H, 5.41, N, 5.00.

**N,N'-Bis(4-n-hexyloxyphenyl)-1,8:4,5-naphthalenetetracarboxylic** (**NBI-4-n-OHePh**), yellow solid, reaction yield of 65%. <sup>1</sup>H NMR (CDCl<sub>3</sub>, 400 MHz, ppm): 8.83 (s, 4H); 7.25-7.22 (d, 4H, J=8.8Hz); 7.09-7.06 (d, 4H, J=8.8 Hz); 4.03 (t, 4H, J = 6,4 Hz); 1.87-1.80 (m, 4H); 1.53–1.46 (m, 4H); 1.39–1.35 (m, 8H); 0.93 (t, 6H, J = 6.8 Hz). <sup>13</sup>C NMR (CDCl<sub>3</sub>, 100 MHz): 163.15; 159.51; 131.37; 129.29; 127.11; 127.00; 126.61; 115.34; 68.26; 31.58; 29.20; 25.74; 22.63; 14.06. FTIR (KBr, cm<sup>-1</sup>): 3465, 3417, 2944, 2872, 1711, 1657, 1507, 1468, 1351, 1237, 1134, 1023, 974, 866, 833, 769, 736. Elemental analysis: Calcd for C<sub>38</sub>H<sub>38</sub>N<sub>2</sub>O<sub>6</sub>: C, 73.77, H, 6.19, N, 4.53. Found: C, 73.75, H, 6.24, N, 4.54.

**N,N'-Bis(4-n-octyloxyphenyl)-1,8:4,5-naphthalenetetracarboxylic** (**NBI-4-n-OOcPh**) was prepared in a form of a yellow solid, reaction yield of 73%. <sup>1</sup>H NMR (CDCl<sub>3</sub>, 400 MHz, ppm): 8,83 (s, 4H); 7.25-7.22 (d, 4H, J=8.8); 7.09-7.06 (m, 4H, J=9.2); 4.03 (t, 4H, J = 6.4 Hz); 1.87-1.79 (m, 4H); 1.53-1.45 (m, 4H); 1.42-1.27 (m, 16H); 0.91 (t, 6H, J = 6.8 Hz). <sup>13</sup>C NMR (CDCl<sub>3</sub>, 100 MHz): 163.16; 159.52; 131.38; 129.30; 127.13; 127.03, 126.63; 115.36; 68.29; 31.84; 29.37; 29.26; 26.08; 22.68; 14.12. FTIR (KBr, cm<sup>-1</sup>): 3465, 3411, 2927, 2851, 2363, 1711,1657, 1576, 1507, 1474, 1389, 1341, 1291, 1237, 1188, 1167, 1038, 980, 839, 763, 737. Elemental analysis: Calcd for  $C_{42}H_{46}N_2O_6$ : C, 74.75, H, 6.82, N, 4.15. Found: C, 74.59, H, 6.82, N, 4.14.

Solution processing. Thin films of the studied semiconductors were deposited on glass or on SiO<sub>2</sub> covered Si substrate by spin-coating or drop-casting. For some structural studies and in the process of transistors fabrication the studied bisimides were deposited by zone-casting, which allows to obtain highly oriented, thin semiconductors layers on large flat surface area.<sup>24-26</sup> In this method a solution of organic semiconductor is continuously supplied onto a moving substrate from a stationary, flat nozzle. In the meniscus formed between the nozzle and the substrate, gradients of concentration and temperature are created due to continuous evaporation of the solvent. These gradients are the driving forces of unidirectional crystallization within the formed layer. The deposition of a uniform, highly ordered layer requires optimization of several parameters for each individual semiconductor being deposited; the main ones are concentration and temperature of the solution, its supply rate, height of the meniscus, temperature of the substrate and its moving speed.

**Spectroscopic characterization**. <sup>1</sup>H and <sup>13</sup>C NMR spectra were registered using a Varian Mercury (400 and 100 MHz, respectively) spectrometer. FTIR spectroscopic investigations were performed using a BIO-RAD FTS-165 spectrometer. Solution and solid state UV-vis-NIR spectra were recorded on a Varian Cary 5000 spectrometer.

**Cycling voltammetry investigations.** Cyclic voltammograms of the synthesized naphtalene bisimides were registered using an Autolab potentiostat (Eco Chemie). The electrolytic medium consisted of the studied bisimide ( $10^{-3}$  M) dissolved in 0.1 M methylene chloride solution of Bu<sub>4</sub>NBF<sub>4</sub>. The measurements were performed in an inert atmosphere, using a platinum working electrode of the surface area of 3 mm<sup>2</sup>, a platinum wire counter electrode and an Ag/0.1 M Ag<sup>+</sup> reference electrode.

**X-ray diffraction studies**. In the case of the investigations of single crystals, the X-ray Crystallography Diffraction data were collected at 150 K using an Oxford - Diffraction X Calibur S Kappa geometry diffractometer (MoK $\alpha$  radiation, graphite monochromator,  $\lambda = 0.71073$  Å). The cell parameters were obtained with intensities detected on  $n_{batch}$  batches of 5 frames. For three settings of  $\phi$  and  $\psi$ ,  $N_{imag}$  narrow data were collected for 11 increments in  $\omega$  with an exposure time  $t_{exp}$ . Unique intensities detected on all frames using the Oxford-diffraction Red program were used to refine the values of cell parameters. The hydrogen atoms were all fixed in ideal positions. The parameters  $N_{imag}$ ,  $n_{batch}$ ,  $t_{exp}$ , the total number of reflections  $N_{tot.refl}$ , the number of independent reflections  $N_{indrefl}$  and the final indices  $R_1$  and  $wR_2$  are all collected in Table 1.

**Table 1** Experimental parameters used for determining the single crystallographic cells of alkoxy-substituted naphthalene bisimides

Molecule	NBI-4n-OBuPh	NBI-4n-OHePh	NBI-4n-OOcPh	
$N_{imag}$	434	493	423	
$n_{batch}$	6	3	6	
$t_{exp}$	220	20	80	
$N_{tot.refl}$	13871	13926	9191	
$N_{indrefl}$	4095	6431	5214	
$R_1$	0.0784	0.0818	0.079	
$wR_2$	0.1054	0.1255	0.1207	

Powder diffractograms were recorded in the reflection (Bragg-Brentano  $\theta/2\theta$  geometry using a Panalatycal powder diffractometer equipped with a Cu K $\alpha$  radiation source ( $\lambda$ = 1.5418 Å) and a divergence slit of 1/4°. The powder was deposited on a crystalline Si substrate to minimize the background contribution of the sample holder. Continuous scans were recorded between 2 and 60° in  $\theta$  during 3h using a X'Celerator detector.

X-ray diffraction studies of thin layers of bisimide semiconductors deposited on glass or  $SiO_2/Si$  substrates were carried out in the same diffraction geometry on a Panalatycal Empyrean diffractometer ( $CoK\alpha_1$  radiation,  $\lambda$ =1.789 Å), equipped with a mirror and a divergence slit of  $1/32^\circ$  on the incoming beam side, Soller slits of  $0.04^\circ$  and a PixCel3D rapid detector used in the 1D scanning mode, on the diffracted beam side. Continuous scans were recorded from  $2^\circ$  to  $60^\circ$  in  $2\theta$  for the total time from 3 to 7 hours, depending on the scattering power of the studied layers.

**Polarized Optical Microscopic studies**. Bisimide layers zone-cast on glass or quartz substrates, were examined using polarized optical microscopy (POM) either in the light transmission or in the reflection mode.

Transistors fabrication and testing. Bottom contact, top gate thin film transistors were prepared in the following manner. Using an appropriate mask from the mask set, a 4 nm chromium layer was first evaporated on a glass substrate, serving as an adhesive layer for gold electrodes. Then, 50 nm thick gold drain and source electrodes were deposited on chromium, resulting in channels of 4 mm width and 30 to 100 µm length. Typically on one glass substrate 18 pairs of drain and source electrodes were patterned. In the next step a solution of a given bisimide in chlorobenzene was zone-cast with the casting direction along the channel length. The deposited layers were then annealed at 100°C for 4 hours with the goal to remove the residual solvent. A 100 nm layer of Parylene C was deposited (see Supplementary Information for details) on the annealed semiconductor active layer which served as a dielectric and a protective layer. In the last step a silver gate electrode was deposited by evaporation in vacuum through a matching shadow mask from the masks set. Output and transfer characteristics of the fabricated transistors were measured in air, using needle electrodes and circuits with voltage/current sources and electrometers (Keithley 2410).

**DFT calculations**. DFT calculations were carried out using Gaussian09 Revision D.01<sup>27</sup> package and employing hybrid B3LYP<sup>28-30</sup> exchange correlation potential combined with 6-31G(d) basis set. Ground-state geometries were fully optimized until a stable local minimum was

found, which was confirmed by normal-mode analysis (no imaginary frequencies were present). Symmetry constrains were put wherever possible imposing either  $C_{2h}$  or  $C_2$  point group. In order to improve numerical accuracy of the calculations two-electron integrals and their derivatives were calculated in a modified way employing the pruned (99,590) integration grid consisting of 99 radial shells and 590 angular points per shell. The ground-state geometries were then optimized in solution using polarizable continuum model (PCM)<sup>31</sup> at the same level of theory with dichloromethane and chloroform as solvents. The oscillator strengths and energies of the vertical singlet excitations were calculated employing time-dependant version (TD) of DFT<sup>32-38</sup> and again at the same level of theory (B3LYP/6-31G(d)) and moreover applying Coulomb-attenuated hybrid exchange-correlation (CAM–B3LYP/6-31G(d)) functional<sup>39</sup> with chloroform as the solvent. The TD-DFT results were retrieved from output files using GaussSum 2.2.<sup>40</sup> The nature of the multiconfigurational transitions was analyzed with natural transition orbitals.<sup>41</sup> Molecular orbital plots were generated from .cube files with Gabedit 2.4.6.<sup>42</sup>

### **Results and discussion**

Electrochemical and spectroscopic studies – experiment *vs* DFT calculations. The studied organic semiconductors are depicted in Scheme 1. They differ only by the length of the solubilizing alkoxy substituent. All three compounds studied are readily soluble in such halo derivatives as dichloromethane, chloroform, chlorobenzene and others.

Similarly as other functionalized naphthalene bisimides, compounds of the NBI-4-n-ORPh family undergo a two-step *quasi*-reversible electrochemical reduction to a radical anion in the first step and to a spinless dianion in the second one.<sup>43</sup> Their voltammetric response in the negative (*vs* Fc/Fc<sup>+</sup>) potentials range is very similar – a representative voltammogram, recorded for NBI-4-n-OOcPh, is shown in Fig. 1 whereas all electrochemical reduction data are collected in Table 2.

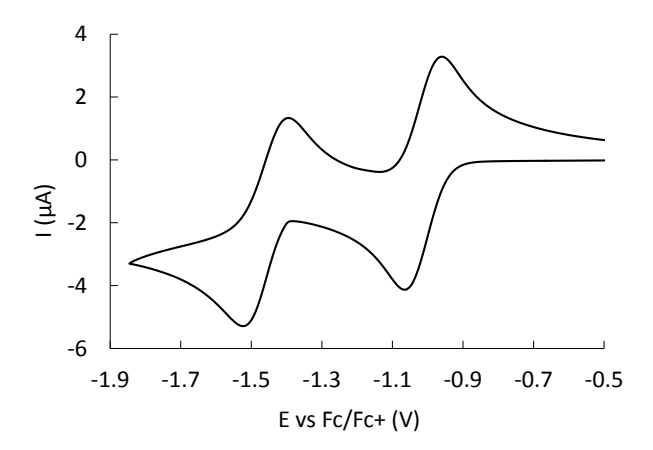


**Fig. 1** Cyclic voltammogram of NBI-4-n-OOcPh (10<sup>-3</sup> M) registered in the negative potentials range. Scan rate 50 mVs<sup>-1</sup>, electrolyte 0.1 M Bu<sub>4</sub>NBF<sub>4</sub> in CH<sub>2</sub>Cl<sub>2</sub>; potentials *vs* ferrocene redox couple.

**Table 2** Redox potentials (vs Fc/Fc<sup>+</sup>) measured for the two-step reduction and irreversible oxidation together electrochemically determined electron affinity (EA) and ionization potential (IP) values for alkoxyphenyl-substituted naphthalene bisimides

Compound	$E_{1red} / V$	$E_{lox} / V$	E <sub>2red</sub> / V	$E_{2ox} / V$	EA  / eV	E <sub>3ox. (onset)</sub> / V	IP / eV
NBI-4-n-OBuPh	-1.07	-0.98	-1.55	-1.42	4.125	1.23	6.33
NBI-4-n-OHePh	-1.06	-0.97	-1.53	-1.41	4.115	1.27	6.37
NBI-4-n-OOcPh	-1.06	-0.96	-1.52	-1.39	4.110	1.26	6.36

In the positive potential range the studied compounds undergo an irreversible oxidation. Only in the case of NBI-4-n-OOcPh a clear oxidation peak can be distinguished (see Fig. 2). For NBI-4-n-OBuPh and NBI-4-n-OHePh the oxidation is manifested by steeply increasing anodic peak without any clear maximum up to the potential of 1.7 V vs. Fc/Fc<sup>+</sup> (not shown). The potentials of the oxidation onsets for all three bisimides are listed in Table 2.

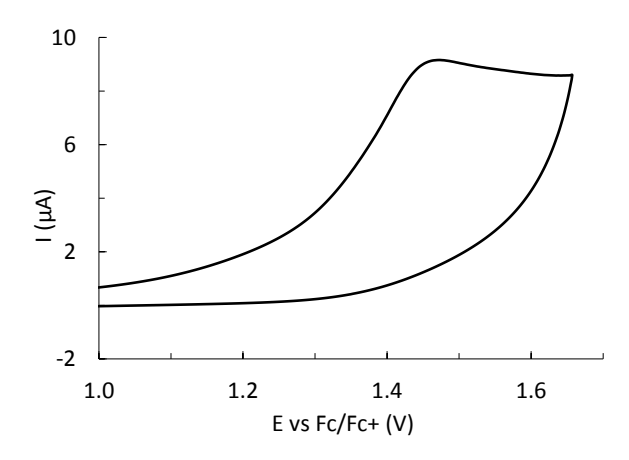


**Fig. 2** Cyclic voltammogram of NBI-4-n-OOcPh (10<sup>-3</sup> M) registered in the positive potential range. Scan rate 50 mVs<sup>-1</sup>, electrolyte 0.1 M Bu<sub>4</sub>NBF<sub>4</sub> in CH<sub>2</sub>Cl<sub>2</sub>; potentials *vs* ferrocene redox couple.

The formal potential of the first redox couple,  $E_1^0 = (E_{1red} + E_{1ox})/2$ , is very close for all compounds studied (in the range from -1.03 V to -1.01 V vs. Fc/Fc<sup>+</sup>). It is significantly higher (by 70 to 130 mV) than the corresponding potential in naphthalene bisimides N-substituted with alkyl groups<sup>18</sup> and very close to the values measured for alkylphenyl substituted naphthalene bisimides.<sup>44</sup> This observation indicates that the LUMO level and, by consequence, the electron affinity (EA) of the molecules studied are not affected by the electron donating/withdrawing properties of the solubilizing substituent. This problem will be discussed later.

To the contrary, the onset of the irreversible oxidation process in alkoxyphenyl N-substituted naphthalene bisimides starts at lower potentials as compared to the case of alkylphenyl-substituted ones.<sup>44</sup>

Electrochemical investigations are of crucial importance for any new organic semiconductor since the measured potentials of its reduction to a radical anion and its oxidation to a radical cation give access to the estimation of its electron affinity (EA) and ionization potential (IP), respectively. The "electrochemical" EA value is calculated using the formal potential of the first redox couple listed in Table 2, *i.e.*  $E_1^0$ , and applying equation (1):

$$EA(eV) = -|e| \cdot (E_1^0 + 5.1)$$
 (1)

In the estimation of EA, the formal redox potential,  $E_1^0$ , must be expressed in the absolute potential scale *i.e.* with respect to the vacuum level. Trasatti attributed a value of -5.1 V in the absolute scale to the formal redox potential of the Fc/Fc<sup>+</sup> couple in non-aqueous electrolytes.<sup>45</sup>

By analogy, the formal redox potential of the couple corresponding to the oxidation of a neutral molecule to a radical cation should be taken for the calculations of the "electrochemical" IP values. As already mentioned, this process in alkoxyphenyl-substituted bisimides is irreversible and yields a rather poorly defined electrochemical answer. Therefore no formal redox potential can be determined for this redox reaction. In such cases frequently the potential of the oxidation peak onset is taken for the calculations. This approach has however to be considered as a rather rough approximation, although in many reversible redox couples the potential of the onset of the oxidation peak is close to the formal redox potential. Following this procedure we have calculated the "electrochemical" IP, using the data collected in Table 3 and applying equation (2):

$$IP(eV) = |e| \cdot (E_{3ox(onset)} + 5.1)$$
 (2)

The values of EA and IP derived from the electrochemical data are collected in Table 2.

A short comment is needed here. In equations (1) and (2) we used the value of -5.1 V as recommended by Trasatti,  $^{45}$  although in the majority of papers a different value (-4.8 V) is attributed to the Fc/Fc<sup>+</sup> couple. Detailed justification for the preferable use of -5.1 V can be found in.  $^{47}$ 

The following predictive messages can be retrieved from the above described electrochemical studies: i) high values of |EA|, in each case exceeding 4.0 eV, make alkoxyphenyl-substituted naphthalene bisimides very promising candidates for the application as active layers in n-channel transistors operating in air, their solution processability constitutes their additional advantage; ii) their IP is also very high (> 6eV), thus they are very stable against oxidation but cannot be used as components of ambipolar transistors or bulk heterojunction photovoltaic cells.

It seems from the electrochemical studies that the effect of the alkoxy substituent on the bisimide reduction is purely inductive in nature since no differences in the first reduction potential are observed for p-R-Ph- $^{44}$  and p-R-O-Ph- derivatives described in this paper. This is

not unexpected because both types of substituents show electron withdrawing character with similar values of the field/inductive, F, parameters<sup>48</sup>. Since the oxidation potential is, in turn, strongly influenced by the presence of the alkoxy group (*vide supra*) it seems that the HOMO and LUMO orbitals must be separated in space, the former being located on the substituent whereas the latter – on the bisimide core. In this respect it is instructive to compare the electrochemical data with the results of DTF calculations which do not only provide the energies, shape and positions of the frontier orbitals but also give access to the EA and IP values. We have carried out such calculations for NBI-4-n-OBuPh.

In the calculations higher-accuracy integration grid was used in order to avoid energy oscillations (possibly due to many  $\rm sp^3$  carbons). Initially, its geometry was constrained to the  $\rm C_{2h}$  symmetry point group and optimized, however the normal mode analysis revealed a second-order stationary point. Therefore, it was repeated, imposing  $\rm C_2$  symmetry. In this case the equilibrium structure was found. In addition to the calculations carried out for vacuum, the geometries of the molecule were also analyzed in chloroform with the goal to compare the theoretical spectrum with the experimental one which was recorded for NBI-4-n-OBuPh dissolved in this solvent. Theoretical investigations were also carried out in dichloromethane – the solvent used in the cyclic voltammetry investigations of NBI-4-n-OBuPh. In this case they were extended to the calculations of the ionization potential (IP) and the electron affinity (EA) as the difference in energy between the radical cation or the radical anion at their equilibrium geometries and the ground-state energy in vacuum and solution.

The frontier orbitals are depicted in Fig. 3. Consistent with the electrochemical findings the HOMO orbitals are located at the phenyloxy segment of the substituent whereas the lobes of LUMO are spread along the central (bisimide) part of the molecule and have an inter-ring bonding character.

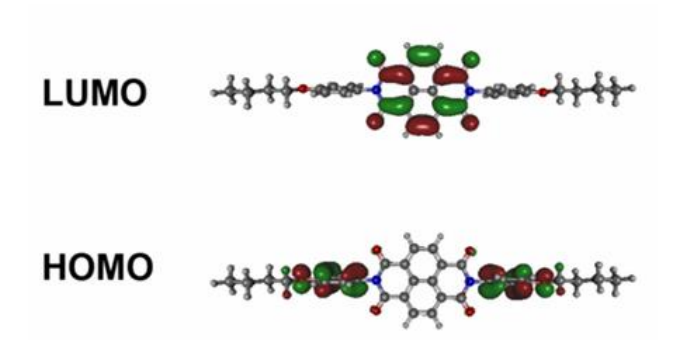


**Fig. 3** Projections of HOMO and LUMO orbitals of NBI-4-n-OBuPh (isovalue = 0.03); green stands for positive and red for negative signs of the wave function.

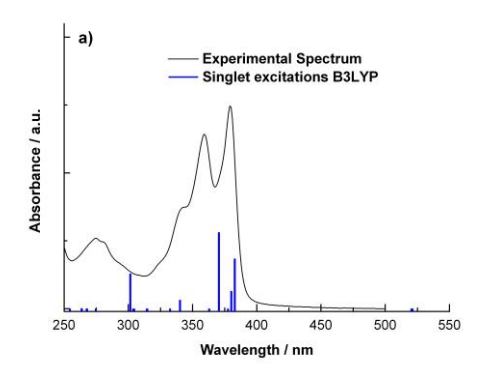
The results of the calculations are collected in Table 3. The values of IP and EA do not match the exact values of HOMO and LUMO because they correspond to equilibrium processes of withdrawing and adding electrons rather than to the simple ground-state analysis. The differences are also clearly seen in the results of the calculations carried out for vacuum and dichloromethane solution, especially in the case of IP and EA. It is therefore obvious that solvent effects must always be taken into account when comparing the calculated and experimental data.

Table 3 Key electronic parameters calculated for NBI-4-n-OBuPh in vacuum and solution

	HOMO / eV	LUMO / eV	$E_g / eV$	IP / eV	EA  / eV
Vacuum	-6.04	-3.23	2.82	6.94	2.02
CH <sub>2</sub> Cl <sub>2</sub>	-6.18	-3.21	2.87	5.51	3.89

The LUMO level (both in vacuum and in solution, *ca.* -3.20 eV) is very close to that calculated for n-butylphenyl substituted naphthalene bisimide (NBI-4-n-BuPh),<sup>44</sup> which is expected taking into account similar inductive effect of the alkoxyphenyl and alkylphenyl substituents on the bisimide core reduction.<sup>48</sup> To the contrary, consistent with the location of the HOMO orbitals, the presence of this group in the substituent strongly influences the position of the HOMO level which is being raised by *ca.* 0.60 eV as compared to the case of NBI-4-n-BuPh.<sup>44</sup> Finally, it should be stated that the same trend is observed in the experimental IP and EA values measured for NBI-4-n-OBuPh in this research and in the data reported for NBI-4-n-BuPh.<sup>44</sup>

UV-vis spectra of all three compounds studied are very similar. In Fig. 4 the spectrum of NBI-4-n-OBuPh is shown as a representative example. In its lower energy part it is dominated by a characteristic strong band of vibronic character with a maximum at 379 nm for the 0-0 transition. This band is attributed to the  $\pi$ - $\pi$ \* transition in the aromatic bisimide core (NBI) as evidenced from the DFT calculations (*vide infra*). In this part of the spectrum naphthalene bisimides N-substituted with alkoxyphenyl groups do not differ from their alkyl-substituted analogues. In the higher energetic part of their spectra an additional peak of lower intensity, possibly showing a vibronic character can be distinguished at 275 nm. This peak is not present in the spectra of alkylphenyl substituted naphthalene bisimides and can tentatively be attributed to a transition in the aromatic substituent modified by the presence of the strongly electrodonating alkoxy group since similar bands are present in low and high molecular weight compounds containing alkoxy-substituted phenyl (phenylene) moieties.



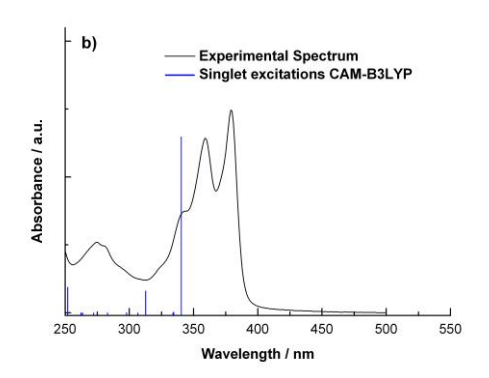


**Fig. 4** Experimental UV-Vis spectrum of NBI-4-n-OBuPh solution in chloroform together with calculated (TD-DFT) vertical transitions of the highest oscillator strength: calculated using a) B3LYP/6-31G(d); b) CAM-B3LYP/6-31G(d).

The theoretical analysis of the UV-Vis spectrum of NBI-4-n-OBuPh was based on the TD-DFT calculations using the molecule geometry optimized (B3LYP) for the chloroform solution and additionally applying CAM-B3LYP on the same geometry for comparison. In order to cover as much of the spectrum as possible, 50 vertical excitations were calculated. They are listed in Table S1 and S2 of Supporting Information. Transitions of the highest oscillator strengths together with the HOMO-LUMO excitation are presented in Table 4, while in Fig. 4 these transitions are compared with the experimental UV-Vis spectrum.

Table 4 Key singlet vertical excitations in NBI-4-n-OBuPh

	Exc. no	$\lambda$ / nm	Osc. strength	Symm.	Contribution	$\lambda_{max}$
B3LYP	1	521.25	0	S-A	H→L (99%)	0.99653
	3	382.81	0.1839	S-B	H-5→L (17%)	
					H-4→L (24%)	0.98903
					H-2→L (58%)	
	4	380.04	0.0649	S-B	H-5→L (79%)	
					H-2→L (16%)	0.97450
	6	370.38	0.2811	S-B	H-4→L (74%)	
					H-2→L (24%)	0.98981
	14	301.50	0.1287	S-B	H-9→L (93%)	0.94151
CAM-B3LYP	1	340.40	0.6484	S-B	H-2→L (96%)	0.98504
	4	312.67	0.0813	S-B	H-5→L (88%)	0.89313
	12	251.96	0.0947	S-B	H-9→L (84%)	0.86518

According to B3LYP the excitation which gives rise to the most intensive band in the spectrum of NBI-4-n-OBuPh does not originate from the HOMO-LUMO transition, which is forbidden. The calculated three transitions of high oscillator strength (transitions 3, 4 and 6 in Table 5) closely match in energy the dominant band in the experimental spectrum of pronounced vibrational structure (0-0 transition at 379 nm). This characteristic band should predominantly originate from the  $\pi$ - $\pi$ \* transition in the bisimide core. However, the NTO analysis of the vertical excitations reveals some contribution from phenylene moieties (note that due to multiconfigurational character of the transitions NTO significantly simplifies the interpretation). The calculations also predict an additional transition of significant oscillator strength in the vicinity of 300 nm. In the experimental spectrum a clear band can be seen in this spectral region. No such band exists in NBI-4-n-BuPh. TD-DFT with CAM-B3LYP using the same geometry provides on the other hand with much clearer picture of the excitations. In this case the pronounced vibronic structure originates exclusively from the highly privileged  $\pi$ - $\pi$ \* transitions on the bisimide core (as confirmed by NTO analysis). Within this XC functional there also exist transitions that give rise to the band in the vicinity of 300 nm. For this reason and what can be

seen for different bisimides of similar structure<sup>2</sup> this approach (CAM-B3LYP) is more robust. Finally, it should be noted that the theoretical calculations are in good agreement with the experimental data.

**X-ray diffraction studies**. \* The capability of forming ordered and, if possible, oriented structures is of crucial importance for potential application of bisimide-based semiconductors as active layers in organic electronics devices. For this reason we have undertaken a detailed study of their crystal structure both in single crystals and in thin layers focusing on the relationship between the processing technique and the resulting supramolecular organization.

We have succeeded in growing single crystals of all three compounds studied. In Fig. 5 a, b and c the crystal packings of NBI-4n-OBuPh, NBI-4n-OHePh and NBI-4n-OOcPh, projected in the (b,c) plane, are compared.

A pronounced effect of the alkyl substituent length on the molecular packing pattern can clearly be noticed. In the unit cell of NBI-4n-OBuPh, molecules form a herring bone arrangement with butyl groups regularly packed along the c axis. The intermolecular distance between the nearest neighbors inside each row is about 0.5 nm. All molecules exhibit a similar conformation with two internal torsion angles between the conjugated core and the substituent phenyl rings of 91 and 70°. With increasing length of the alkyl groups, their conformation becomes more extended, favoring a regular stacking of the molecules in the unit cell. For NBI-4n-OHePh, the adjacent bisimide cores are slightly shifted relatively to each other, which results in a shorter stacking distance of 0.48 nm. The two internal core/phenyl substituent torsion angles are in this case 58 and 72°. They however alternate in the two consecutive molecules along the b axis, still giving two independent molecules per unit cell. In NBI-4n-OOcPh, the inter-alkyl interactions impose the same relatively extended conformation of the molecules as in the case of NBI-4n-OHePh but with only one molecule per unit cell. In each molecule, the phenyl substituents are rotated by 97° with respect to the conjugated core. A stacking mode in which the conjugated core and the phenyl substituents alternatively face each other along the b axis is obtained. The closest distance between the conjugated cores of molecules is around 0.55 nm.

<sup>\*</sup>The supplementary crystallographic data for the compounds discussed in this paper can be found under the following CCDC numbers: i) CCDC 972316 for NBI-4n-OBuPh; ii) CCDC 972318 for NBI-4n-OHePh; iii) CCDC 972 317 for NBI-4n-OOcPh. These data can be obtained free of charge from the Cambridge Crystallographic Data Centre *via* www.ccdc.ac.uk/data\_request/cif

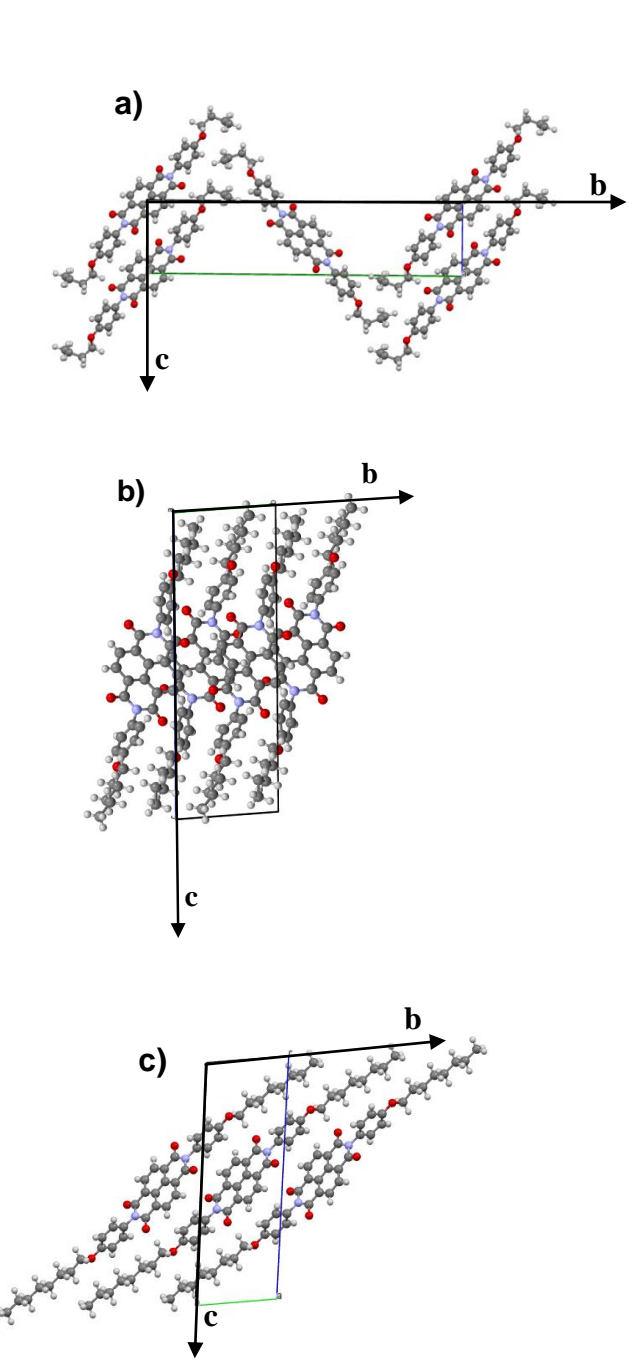


**Fig. 5** Projections in the (b,c) plane of crystallographic structures of a) NBI-4n-OBuPh, monoclinic (space group P2<sub>1</sub>/c), Z = 2, a = 5.0423(4) Å, b = 33.7458(18) Å, c = 7.9966(4) Å,  $β = 100.002(5)^\circ$ , b) NBI-4n-OHePh, triclinic (space group P-1), Z = 2, a = 8.4404(13) Å, b = 8.8932(14) Å, c = 24.019(3) Å,  $α = 89.090(11)^\circ$ ,  $β = 80.490(11)^\circ$ ,  $γ = 62.786(16)^\circ$ , c = 22.3732(18) Å,  $α = 96.434(6)^\circ$ ,  $β = 95.114(7)^\circ$ ,  $γ = 100.318(7)^\circ$ .

In as prepared powders of NBI-4n-OHePh and NBI-4n-OOcPh the crystal structure turned out to be the same as in single crystals since the powder diffractograms calculated from the single crystal data satisfactorily matched the experimental ones. NBI-4n-OBuPh required, however, some additional purification because as prepared powders of this compound, *i.e.* precipitated from the reaction medium and then recrystallized, showed a small admixture of a phase of different crystallographic parameters.

All three naphthalene bisimides are solution processable and can be deposited in a form of thin layers on a variety of substrates. The resulting supramolecular organization as well as the degree of the molecules orientation in the layer depends mainly on the selected processing technique and the type of the substrate used but also on the concentration of the solution, temperature of solvent evaporation and others.

The effect of the substrate can be illustrated by comparing Bragg-Brentano diffractograms of NBI-4n-OBuPh thin layers deposited on SiO<sub>2</sub> covered Si and on glass (see Fig. 6). On glass one broad peak centered at 2.5 nm is obtained whereas on SiO<sub>2</sub>/Si an additional peak at 1.94 nm is present. It is instructive to comment on the 2.5 nm interlayer distance derived from both diffractograms in the context of the single crystal structure. The maximum length of a NBI-4n-OBuPh in its conformational state present in the single crystal is *ca.* 2.5 nm (length measured between the two terminal methyl groups). This may suggest that there exist crystallites in the layer, in which the molecules stand almost perpendicular to the substrate. In the layer deposited on glass this is the only crystalline phase. The period of 1.94 nm, registered for the layer deposited on SiO<sub>2</sub> can be interpreted as originating from crystallites in which the semiconductor molecules form a tilt angle of 55-60° with respect to the substrate. This is also a typical tilt angle which is formed by one of two independent molecules with respect to the b axis in the single crystal structure. Thus, two types of differently oriented crystallite co-exist in this layer. The spin-coated layer are very thin (*ca.* 20 nm, as evaluated from the FWHM value of the peak and applying the Scherrer formula).

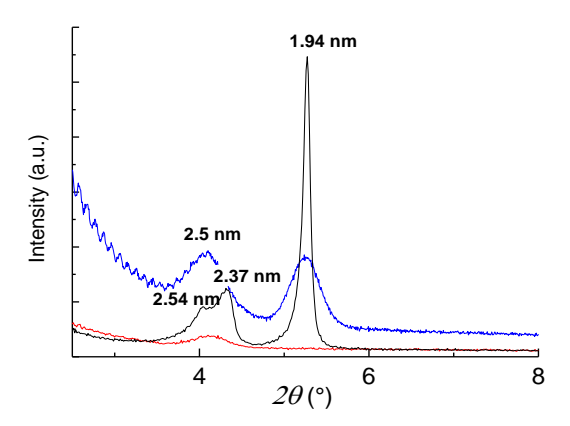


**Fig. 6** Main features of X-ray diffractograms obtained for NBI-4n-OBuPh layers deposited on: SiO<sub>2</sub> covered Si by spin-coating (blue); glass by spin-coating (red); glass by drop-casting (black). Fringes on the blue profile originate from the reflectivity of a thin SiO<sub>2</sub> layer on Si crystal.

Drop-casting on glass yields somehow different diffractograms from those obtained for spin-coated films (see Fig. 6). Three co-existing Bragg reflections (2.54 nm, 2.37 nm and 1.94 nm) can be distinguished in this case corresponding to crystallites in which molecules are differently oriented with respect to the substrate. The FWHM value of the reflection at 1.94 nm (corresponding to the molecules tilted by  $55-60^{\circ}$  with respect to the substrate) yields a coherence length of ca. 100 nm, which corresponds to the average size of the nanocrystals lying of the substrate's surface.

The diffractograms of the films obtained by zone-casting are of special interest since this processing technique was used in the fabrication of transistors. A typical diffractogram obtained of a layer of NBI-4n-OBuPh zone-cast on glass is shown in Fig. 7. In principle, it resembles the diffractogram registered for the drop-cast layer with two broad peaks in the range of 2.55 nm – 2.30 nm and a very thin reflection centered at 1.94 nm. The coherence length, calculated from the FWHM value of the 1.94 nm reflection, is 93 nm which means that these oriented crystals are similar in size as those obtained by drop-casting. Similarly as in drop-cast layers they co-exist with much thinner layers (*ca.* 20 nm) of molecules whose orientation is different.

As already mentioned, NBI-4n-OHePh and NBI-4n-OOcPh adopt a regular stacking sequence in their 3D crystallographic structure with alkyl substituent in their most extended conformation (see Fig. 5). These structural features should therefore facilitate the formation of highly ordered and oriented layers by solution processing.

Representative diffractograms of NBI-4n-OHePh layers spin-coated on SiO<sub>2</sub> and on glass are shown in Fig. 8. They are very similar and show one broad reflection centered at 2.41 nm. In both cases uniform thin layers of the thickness of *ca.* 30 nm (evaluated from the FWHM of the peak and by applying the Scherrer formula) are obtained in which the molecules are uniformly stacked within this period.

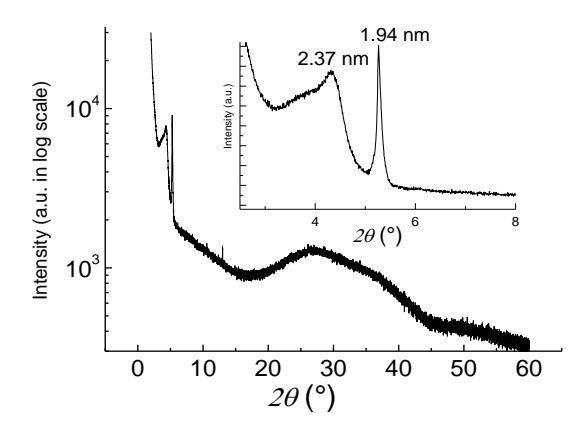
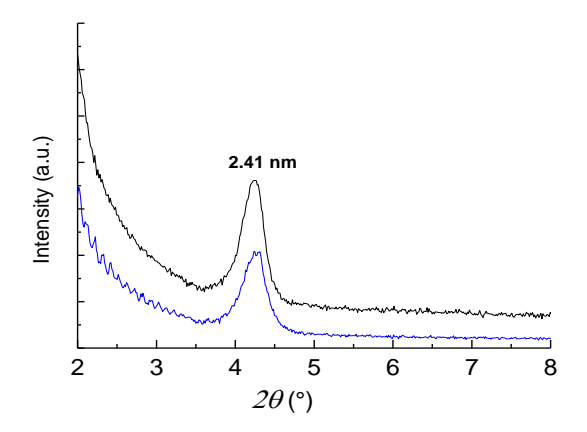


Fig. 7 X-ray diffractogram of a NBI-4n-OBuPh layer, zone-cast on glass.

The length of the molecule in its extended conformation adopted in the single crystal (Fig. 5) is 3.229 nm. The molecule is tilted with respect to the b axis by an angle of ca 50°. Projection of this molecule on a direction perpendicular to the b axis yields 3.229 x sin 50° = 2.47 nm. This value is in a very good agreement with the period found for the thin layer. Upon deposition of the thin layer the substrate compels individual molecules to be tilted and aligned in a row, without any translational shift along the stacking directions. Accordingly, we can consider that the resulting mutual orientation of the molecules is very similar to that found in the single crystal.

In the diffractogram of a zone-cast layer a slightly lower period is found (2.354 nm) compared to that measured for the spin-coated layer. However this layer is thicker and yields a coherence length of 138 nm, calculated from the FWHM value of the 001 reflection. A high degree of the molecules orientation is manifested by the presence of the reflections of higher order, up to 009 (see Fig. 9).



**Fig. 8** Main features of X–ray diffractograms obtained for NBI-4n-OHePh layers spin-coated on: SiO<sub>2</sub> (blue); glass (black). Fringes on the blue profile originate from the reflectivity of thermal SiO<sub>2</sub> layer on Si crystal.

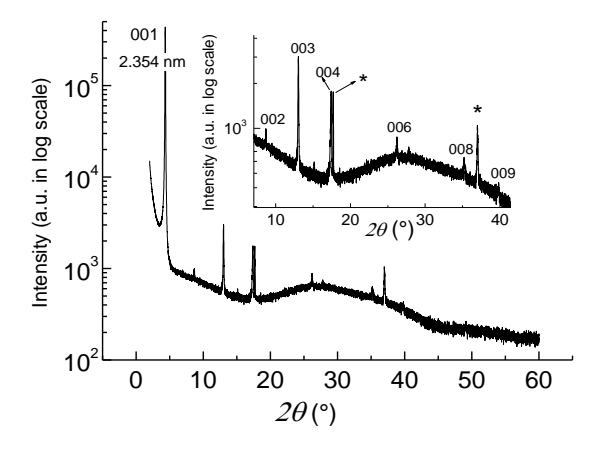


**Fig. 9** X—ray diffractogram obtained for a NBI-4n-OHePh layer zone-cast on glass. Stars indicate peaks which cannot be indexed in the 00l series.

Spin-coated layers of NBI-4n-OOcPh yield two types of diffractograms with either one or two reflections (see Fig. 10). One reflection at 2.61 nm is observed for films deposited on glass whereas for films deposited on SiO<sub>2</sub> an additional peak can be noticed at 2.24 nm, which shows much smaller FWHM.

The length of a NBI-4n-OOcPh molecule in its conformation adopted in the single crystal is 3.684 nm. Applying the same reasoning as in the case of NBI-4n-OHePh a tilt angle of 47° can be found which gives a projected distance of 2.69 nm in the single crystal, very close to the

stacking distance of 2.61 nm found in the thin layers. Thus, in this case again the stacking pattern of the molecules with respect to the substrate resembles that determined for the single crystal.

The presence of the second peak in thin films spin-coated on SiO<sub>2</sub> can be considered as a sign of the coexistence of the zones of oriented tilted molecules with 3D crystals which are surface contacted through the (a,b) plane since this peak can be attributed to the 001 reflection in the direction perpendicular to the substrate. This co-existence of two different phases can be clearly observed in optical microscope images in polarized and nonpolarized light which show alternation of large, structurally and optically homogeneous domains with domains of different optical feature originating from different packing patterns (see Fig. S1 and S2 in Supplementary Information).

A representative diffractogram of a NBI-4n-OOcPH deposited on glass by zone-casting is shown in Fig. 11. A periodic stacking of 2.6 nm is also observed in this case with a coherence length of 150 nm. The presence of higher order reflections (up to 10<sup>th</sup> order) clearly shows a high degree of the molecules alignment in the deposited layer.

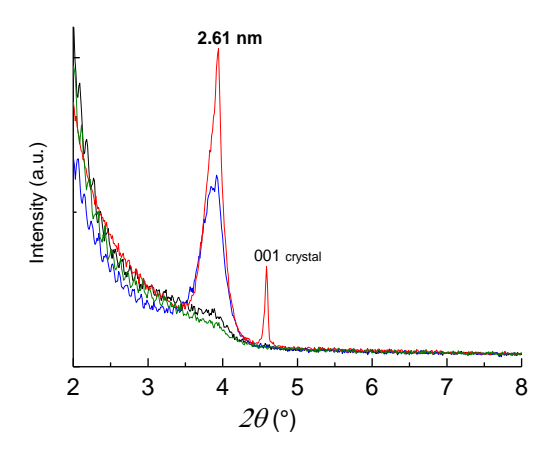


**Fig. 10** X–ray diffractograms of NBI-4n-OOcPH layers deposited from a chloroform solution (c = 10mg/mL) by spin-coating on: native SiO<sub>2</sub> on Si wafer (red) and thermal SiO<sub>2</sub> on Si wafer (blue). Deposited from a chloroform solution (c = 2mg/mL) on thermal SiO<sub>2</sub> on Si wafer (green) and from a chlorobenzene saturated solution on thermal SiO<sub>2</sub> layer on Si wafer (black). Fringes originate from the reflectivity of thermal SiO<sub>2</sub> layer.

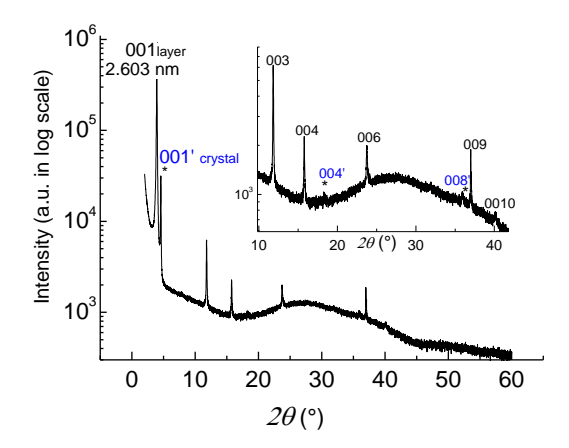


**Fig. 11** X-ray diffractogram of a NBI-4n-OOcPh layer zone-cast on glass. 00l lines indicated in blue originate from crystals whose (a,b) plane is preferentially oriented parallel to the substrate.

To summarize this part of the paper, all three compounds studied adopt in thin layers regular stacking modes. This effect is more pronounced for hexyloxy and octyloxy substituted bisimides. Zone-cast layers are much thicker as compared to spin-coated or drop-cast ones, however they show a very regular supramolecular organization characterized by a very high coherence length. In all cases, several types of oriented crystals are found in the samples. However, in the zone-cast samples of hexyloxy and octyloxy substituted bisimides the best structural homogeneity is found.

Application in n-channel field effect transistors (FETs). Detailed studies of alkoxyphenyl substituted naphthalene bisimides unequivocally show that these compounds combine facile synthesis and solution processability with redox properties predicting their air operating in the n-channel field effect configuration. Moreover, the hexyloxy and octyloxy derivatives (and to a lesser extent the butyloxy one) have a strong tendency to form oriented layers via solution processing. This property is even further enhanced if zone-casting is applied as a processing technique. In this last case, rows of  $\pi$ -stacked molecules are formed with the  $\pi$ -stacking direction parallel to the surface of the substrate. Such orientation of molecules is favorable for electrical charge transport in the bottom contact top gate transistor configuration. We have demonstrated it in one of our previous papers where we showed that the transistors fabricated by zone-casting exhibited almost three orders of magnitude higher electron mobility  $^{21}$  than those in which the active layer was deposited by spin-coating.  $^{18}$ 

The selection of the used dielectric material (Parylene C) requires a short comment. A large variety of organic, inorganic and hybrid (organic/inorganic) dielectrics have been tested in organic field effect transistors (OFETs)<sup>51</sup>. The use of purely inorganic dielectrics and some of hybrid ones is virtually impossible or at least extremely difficult in the fabrication of bottom contact—top gate transistors by solution processing. Therefore, in our research we limited ourselves to the application of solution processable, preferably polymeric dielectrics, due to their film forming properties. Commercially available fluorinated polymer, CYTOP, is a popular choice of a dielectric for both n- and p-channel field transistors and initially we also used it<sup>18, 44</sup>. However in the process of optimizing the device fabrication we found that n-channel transistors with a Parylene C dielectric layer exhibited better parameters (threshold voltage, charge carriers mobility) as compared to those in which CYTOP served as a dielectric, especially for transistors with zone-cast active layer.<sup>21</sup> For these reasons we started to use Parylene C.

In Fig. 12 representative transfer and output characteristics are shown for a transistor with an active layer consisting of zone-cast NBI-4n-OOcPh. The charge carrier mobility,  $\mu$ , the threshold voltage,  $V_{th}$  and the ON/OFF ratio were calculated from the saturation regime, using the following equations (3) and (4):<sup>52,53</sup>

$$\mu = \frac{2L}{WC} \left( \frac{\delta \sqrt{I_d}}{\delta V_g} \right) \tag{3}$$

$$\frac{ON}{OFF} = \frac{I_{d \text{ max}}}{I_{d \text{ min}}} \tag{4}$$

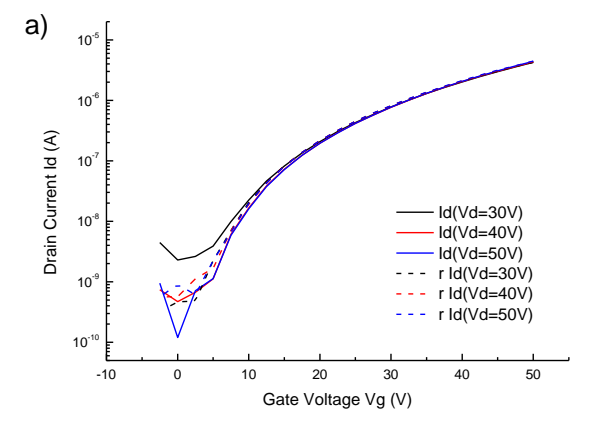
where L is the channel length, W is the channel width, C is the dielectric capacitance per unit area,  $I_d$  is the drain source current, and  $V_g$  is the gate voltage.

The determined parameters for transistors fabricated from all three compounds studied are collected in Table 5. The best charge carriers mobility and the highest ON/OF ratio was obtained for the transistor in which the active layer consisted of NBI-4-n-OOcPh. This is not unexpected since zone-cast layers of this semiconductor showed in the X-ray studies, a supramolecular organization very favorable for charge carriers transport.

Based on high values of |EA| air operating of the transistors fabricated from the bisimides studied could be predicted. In order to examine the working stability of these devices, their characteristics were measured every seven days during four weeks. They were constantly kept at room temperature in air with humidity higher than 40%. It was found that the charge carrier mobility calculated from the transistor characteristics decreased *ca*. 5 times during the first week and then stabilized, without further decrease. In Supplementary Information (Figure S3) the evolution of the charge carriers mobility with the time of exposure is shown.

**Table 5** Field-effect characteristics of transistors with alkoxyphenyl N-substituted naphthalene bisimides as active layers. Measurements performed in air

Compound	$\mu / cm^2 V^{-1} s^{-1}$	$V_{th} / V$	ON/OFF ratio
NBI-4-n-OBuPh	0.0086	5.45	$3.2 \times 10^{2}$
NBI-4-n-OHePh	0.0040	14.1	$2.8 \times 10^{3}$
NBI-4-n-OOcPh	0.049	14.9	$4.7\times10^3$



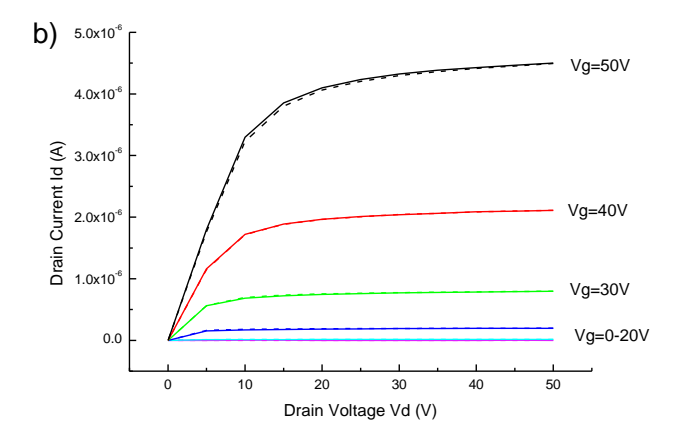


**Fig. 12** Transfer (a) and output (b) characteristics registered for an organic field effect transistor (OFET) with a NBI-4-n-OOcPh active layer, deposited by zone-casting. Forward sweep – solid line; backward sweep – dashed line.

### **Conclusions**

To summarize, we have demonstrated that naphthalene bisimides N-substituted with alkoxyphenyl groups exhibit very interesting redox and structural properties as far as their application in organic electronics is concerned. When solution processed they show a strong tendency to form supramolecularly ordered and oriented thin layers which is further enhanced by application of the zone-casting technique. Moreover, their high |EA| makes them suitable candidates for fabricating n-channel FETs. Such transistors fabricated by solution processing show good electrical transport parameters and can operate in air even unprotected. Long term stability tests in ambient conditions show that after the initial period of the charge carriers mobility decease their electrical parameters stabilize.

### **Author Information**

### **Corresponding Authors**

\*e-mail: zagorska@ch.pw.edu.pl; \*\*e-mail: apron@ch.pw.edu.pl

### Acknowledgement

The presented research was financed by the project entitled "New solution processable organic and hybrid (organic/inorganic) functional materials for electronics, optoelectronics and spintronics" (Contract No. TEAM/2011–8/6), which is operated within the Foundation for the Polish Science Team Programme, confinanced by the EU European Regional Development Fund (L.S., D.W., M.Z. and A.P.). R.R. additionally acknowledges the support of the Foundation for Polish Science within the framework of START 2013 Programme. I.T. wants to acknowledge the Grant 2012/07/B/ST8/03789 of the Polish National Science Centre (NCN). J.Z. thanks for financial support provided by the International PhD Projects Programme of the Foundation for Polish Science, cofinanced from the European Regional Development Fund within the innovative Economy Operational Programme "Grants for Innovation". The Gaussian09 calculations were carried out in the Wroclaw Centre for Networking and Supercomputing, WCSS, Wroclaw, Poland. (http://www.wcss.wroc.pl), under calculational Grant No. 283.

### **Notes**

**Electronic supplementary information (ESI) available:** Experimental and DFT calculation details, polarized optical microscopy images, evolution of the electron mobility with time.

### References

- 1 V. B. Sheshanath, H. J. Chintan and J. L. Steven, *Chem. Soc. Rev.*, 2008, 37, 331.
- 2 R. Rybakiewicz, J. Zapala, D. Djurado, R. Nowakowski, P. Toman, J. Pfleger, J.–M. Verilhac, M. Zagorska and A. Pron, *Phys. Chem. Chem. Phys.*, 2013, **15**, 1578.
- R. Rybakiewicz, D. Djurado, H. Cybulski, E. Dobrzynska, I. Kulszewicz-Bajer, D. Boudinet, J.–M. Verilhac, M. Zagorska and A. Pron, *Synth. Met.*, 2011, **161**, 1600.
- Z. Chen, A. Lohr, C. R. Saha-Möller and R. Würthner, Chem. Soc. Rev., 2009, 38, 564.
- 5 N. Sokolov, M. E. Roberts, O. B. Johnson, Y. Cao and Z. Bao, *Adv. Mater.*, 2010, **22**, 2349.
- J. E. Anthony, A. Facchetti, M. Heeney, S. R. Marder and X. Zhan, *Adv. Mater.*, 2010, 22, 3876.

- 7 X. Zhan, A. Facchetti, S. Barlow, T. J. Marks, M. A. Ratner and M. R. Wasielewski, *Adv. Mater.*, 2011, **23**, 268.
- 8 F. Würthner and M. Stolte, *Chem. Commun.*, 2011, **47**, 5109.
- 9 C. Huang, S. Barlow and S. R. Marder, *J. Org. Chem.*, 2011, **76**, 2386.
- 10 Y. Kim, J. Hong, J. Hak Oh and C. Yang, *Chem. Mater.*, 2013, **25**, 3251.
- 11 C. Gu, W. Hu, J. Yao and H. Fu, Chem. Mater., 2013, 25, 2178.
- 12 A. Pron, R. R. Reghu, R. Rybakiewicz, H. Cybulski, D. Djurado, J. V. Grazulevicius, M. Zagorska, I. Kulszewicz-Bajer and J.-M. Verilhac, *J. Phys. Chem. C*, 2011, **115**, 15008.
- A. Pron. P. Gawrys, M. Zagorska, D. Djurado and R. Demadrille, *Chem Soc Rev.*, 2010, **39**, 2577.
- 14 P. Bujak, I. Kulszewicz-Bajer, M. Zagorska, V. Maurel, I. Wielgus and A. Pron, *Chem. Soc. Rev.*, 2013, **42**, 8895.
- 15 R. Schmidt, J. H. Oh, Y.-S. Sun, M. Deppisch, A.-M. Krause, K. Radacki, H. Braunschweig, M. Könemann, P. Erk, Z. Bao and F. Würthner, *J. Am.* Chem. Soc., 2009, **131**, 6215.
- H. E. Katz, A. J. Lovinger, J. Johnson, C. Kloc, T. Siegrist, W. Li, Y. Y. Lin and A. Dodabalapur, *Nature*, 2000, 404, 478.
- 17 H. E. Katz, J. Johnson, A. J. Lovinger and W. J. Li, *J. Am. Chem. Soc.*, 2000, **122**, 7787.
- P. Gawrys, D. Boudinet, M. Zagorska, D. Djurado, J.-M. Verilhac, G. Horowitz, J. Pecaud, S. Pouget and A. Pron, *Synth. Met.*, 2009, **159**, 1478.
- 19 M.-M. Shi, H.-Z. Chen, J.-Z. Sun, J. Ye and M. Wang, *Chem. Commun.*, 2003, **14**, 1710.
- 20 H. Z. Chen, M. M. Ling, X. Mo, M. M. Shi, M. Wang and Z. Bao, *Chem. Mater.*, 2007, **19**, 816.
- I. Tszydel, M. Kucinska, T. Marszalek, R. Rybakiewicz, A. Nosal, J. Jung, M. Gazicki-Lipman, C. Pitsalidis, C. Gravalidis, C. Logothetidis, M. Zagorska and J. Ulanski, *Adv. Funct. Mat.*, 2012, **22**, 3840.
- W. S. C. Roelofs, S. G. J. Mathijssen, J. C. Bijleveld, D. Raiteri, T. C. T. Geuns, M. Kemerink, E. Cantatore, R. A. J. Janssen and D. M. Leeuw, *Appl. Phys. Lett.*, 2011, **98**, 203301.
- 23 S. Fomine, L. Fomina, R. Arreola and J. Carlos Alonso, *Polymer*, 1999, **40**, 2051.

- P. Miskiewicz, M. Mas-Torrent, J. Jung, S. Kotarba, I. Glowacki, E. Gomar–Nadal, D. B. Amabilino, J. Veciana, B. Krause, D. Carbone, C. Rovira and J. Ulanski, *Chem. Mater.*, 2006, **18**, 4724.
- W. Pisula, A. Menon, M. Stepputat, I. Lieberwirth, U. Kolb, A. Tracz, H. Sirringhaus, T. Pakula and K. Muellen, *Adv. Mater.*, 2005, **6**, 684.
- 26 Y. Su, X. Gao, J. Liu, R. Xing and Y. Han, Phys. Chem. Chem. Phys., 2013, 15, 14396.
- M. J. Frisch, G. W. Trucks, H. B. Schlegel, G. E. Scuseria, M. A. Robb, J. R. Cheeseman, G. Scalmani, V. Barone, B. Mennucci, G. A. Petersson, H. Nakatsuji, M. Caricato, X. Li, H. P. Hratchian, A. F. Izmaylov, J. Bloino, G. Zheng, J. L. Sonnenberg, M. Hada, M. Ehara, K. Toyota, R. Fukuda, J. Hasegawa, M. Ishida, T. Nakajima, Y. Honda, O. Kitao, H. Nakai, T. Vreven, J. A. Montgomery, Jr., J. E. Peralta, F. Ogliaro, M. Bearpark, J. J. Heyd, E. Brothers, K. N. Kudin, V. N. Staroverov, T. Keith, R. Kobayashi, J. Normand, K. Raghavachari, A. Rendell, J. C. Burant, S. S. Iyengar, J. Tomasi, M. Cossi, N. Rega, J. M. Millam, M. Klene, J. E. Knox, J. B. Cross, V. Bakken, C. Adamo, J. Jaramillo, R. Gomperts, R. E. Stratmann, O. Yazyev, A. J. Austin, R. Cammi, C. Pomelli, J. W. Ochterski, R. L. Martin, K. Morokuma, V. G. Zakrzewski, G. A. Voth, P. Salvador, S. Dannenberg, A. D. Dapprich, O. Daniels, J. B. Farkas, J. V. Foresman, J. Ortiz, J. Cioslowski and D. J. Fox, *Gaussian 09, Revision D.01*, Gaussian, Inc., Wallingford CT, 2013.
- 28 A. D. Becke, J. Chem. Phys., 1993, 98, 1372.
- 29 A. D. Becke, *J. Chem. Phys.*, 1993, **98**, 5648.
- 30 C. T. Lee, W. T. Yang and R. G. Parr, *Phys. Rev. B*, 1988, **37**, 785.
- 31 J. Tomasi, B. Mennucci and R. Cammi, *Chem. Rev.*, 2005, **105**, 2999.
- 32 R. Bauernschmitt and R. Ahlrichs, Chem. Phys. Lett., 1996, 254, 454.
- 33 M. E. Casida, C. Jamorski, K. C. Casida and D. R. Salahub, *J. Chem. Phys.*, 1998, 108, 4439.
- 34 R. E. Stratmann, G. E. Scuseria and M. J. Frisch, *J. Chem. Phys.*, 1998, **109**, 8218.
- 35 C. V. Caillie and R. D. Amos, *Chem. Phys.*, *Lett.*, 1999, **308**, 249-55.
- 36 C. V. Caillie and R. D. Amos, *Chem. Phys.*, *Lett.*, 2000, **317**, 159.
- 37 F. Furche and R. Ahlrichs, *J. Chem. Phys.*, 2002, **117**, 7433.

- 38 G. Scalmani, M. J. Frisch, B. Mennucci, J. Tomasi, R. Cammi and V. Barone, *J. Chem. Phys.*, 2006, **124**, 1.
- 39 T. Yanai, D. Tew and N. Handy, Chem. Phys. Lett., 2004, 393, 51
- 40 N. M. O'Boyle, A. L. Tenderholt and K. M. Langner, *J. Comput. Chem.*, 2008, **29**, 839.
- 41 R. L. Martin, J. Chem. Phys., 2003, 118, 4775
- 42 A.-R. Allouche, J. Comput. Chem., 2011, 32, 174.
- 43 S. K. Lee, Y. Zu, A. Herrmann, Y. Geerts, K. Mullen and A. J. Bard, *J. Am. Chem. Soc.*, 1999, **121**, 3513.
- P. Gawrys, D. Djurado, J. R. Rimarcik, A. Kornet, D. Boudinet, J.-M. Verilhac, V. Lukes, I. Wielgus, M. Zagorska, and A. Pron, *J. Phys. Chem. B*, 2010, **114**, 1803.
- 45 S. Trasatti, Pure & Appl Chem., 1986, **58**, 955.
- 46 R. Rybakiewicz, P. Gawrys, D. Tsikritzis, K. Emmanouil, S. Kennou, M. Zagorska and A. Pron, *Electrochim. Acta*, 2013, **96**, 13.
- 47 C. M. Cardona, W. Li, A. E. Kaifer, D. Stockdale and G. C. Bazan, *Adv. Mater.*, 2011, **23**, 2367.
- 48 C. Hansch, A. Leo and W. Taft, *Chem. Rev.*, 1991, **91**, 165.
- 49 L. X. Song, H. M. Wang, X. Q. Guo and L. Bai, J. Org. Chem., 2008, 73, 8305.
- 50 B.Yu, Y. Gao and H. Li, *J. Appl. Polym. Sci.*, 2004, **91**, 425.
- 51 R. P. Ortiz, A. Facchetti and T.J. Marks, Chem. Rev., 2010, 110, 205.
- S. Y. Cho, J. M. Ko, J.-M. Jung, J. Y. Lee, D. H. Choi and C. Lee, *Org. Electron.*, 2012, 13, 1329.
- H. Yan, Z. Chen, Y. Zheng, C. Newman, J. R. Quinn, F. Dotz, M. Kastler and A. Facchetti, *Nature*, 2009, **457**, 679.